THE ASTRONOMICAL JOURNAL, 121:2549–2556, 2001 May
© 2001. The American Astronomical Society. All rights reserved. Printed in U.S.A.

HUBBLE SPACE TELESCOPE NICMOS IMAGING OF THE CORES OF M31 AND M32

MICHAEL R. CORBIN, EARL O'NEIL, AND MARCIA J. RIEKE
NICMOS Group, Steward Observatory, University of Arizona, 933 North Cherry Avenue, Tucson, AZ 85721; mcorbin@as.arizona.edu
Received 2000 December 11; accepted 2001 February 14

ABSTRACT

We present 1.1, 1.6, and 2.2 μm images of the cores of the Local Group galaxies M31 and M32 obtained with the Near Infrared Camera and Multi-Object Spectrometer of the *Hubble Space Telescope* (*HST*). These images are also compared with optical images of the galaxies obtained with the *HST* Wide Field Planetary Camera 2 (WFPC2). In M31, the nucleus remains distinctly asymmetric in all of the infrared bands, with no evidence of concentrated dust, although the distinction between the two nuclei, P1 and P2, is not as strong as in the WFPC2 and earlier WF/PC-1 images. This result is nonetheless consistent with the model of the nucleus as an eccentric stellar disk produced by the dynamical influence of a central supermassive black hole. Several individual M giant stars are detected within $\sim 3''$ of the nuclei and may represent stars that have escaped from the disk and phase-mixed around the nuclear center of mass. In M32 we also do not find strong evidence of dust, and the brightness profiles within the central $\sim 1''$ of the infrared images can be fitted by a power law of the same form as that fitted to the optical images. The infrared color profiles of the central few arcseconds of M32 show no strong gradients and indicate a population dominated by K giant stars. This is consistent with recent ground-based spectroscopy and photometry of the core region, which similarly show no strong gradients in age or metallicity within its stellar population.

Key words: galaxies: individual (M31, M32) — galaxies: nuclei — galaxies: photometry — infrared radiation

1. INTRODUCTION

Observations of the Andromeda galaxy (M31) and its companion M32 with the *Hubble Space Telescope* (*HST*) have yielded remarkable results. Imaging of the core of M31 with the Wide Field Planetary Cameras (WF/PC-1 and WFPC2) has revealed it to consist of two nuclei, the optically brighter P1 and the fainter P2 to the southwest, with a compact but resolved ultraviolet source lying at P2's northeastern edge (Lauer et al. 1993; King, Stanford, & Crane 1995; Lauer et al. 1998, hereafter L98). While M32 has a single nucleus, its brightness profile is sharply peaked, indicating a strong increase in the stellar density within the inner ~ 1 pc, likely caused by a massive black hole. Studies of the stellar kinematics within $0''.1$ of M32's nucleus with the *HST* Faint Object Spectrograph have supported this interpretation, revealing a high velocity dispersion ($\simeq 150$ km s^{-1}) indicative of a black hole of mass $\sim 3 \times 10^6\ M_\odot$ (van der Marel, de Zeeuw, & Rix 1997; van der Marel et al. 1998). Similarly, *HST* and ground-based spectroscopy of M31's nuclei (Kormendy & Bender 1999; Statler et al. 1999) have generally supported the model of Tremaine (1995), in which the double nuclei are the result of the dynamical influence of a supermassive ($\sim 3 \times 10^7\ M_\odot$) black hole on the kinematics of the surrounding stars, specifically, causing them to form a highly eccentric disk with the hole at the dynamical center.

Despite the rich detail of these observational results, several important questions remain. In particular, the influence of dust on the ultraviolet and optical morphologies of the cores of both galaxies remains uncertain, as does the level at which their respective black holes are accreting material. For M31, while the images of Lauer et al. (1993), King et al. (1995), Brown et al. (1998), and L98 clearly show two distinct nuclei, it is of interest to see if and how the morphology of these nuclei changes in the near-infrared, which is more transparent to dust and better traces the evolved stars in the region. For M32, it is similarly of interest to see whether the form of the optical brightness profile found by L98 is the same in the near-infrared, and whether the lack of a strong color gradient seen in the ground-based infrared images of Peletier (1993) continues to the subarcsecond scale. Weak nuclear activity in M32 is suggested on the basis of *ROSAT* and *ASCA* X-ray satellite observations (Eskridge, White, & Davis 1996; Lowenstein et al. 1998; Zang & Meurs 1999), and by a possible excess of emission in the far-ultraviolet (Ohl et al. 1998). The stellar populations of the cores of both galaxies are also incompletely probed by the available ultraviolet and optical data (L98; Brown et al. 1998, 2000; Kormendy & Bender 1999), which may select against their coolest stars.

These issues motivated us to obtain broadband images of the inner $\sim 19''$ of both galaxies with the *HST* Near Infrared Camera and Multi-Object Spectrometer (NICMOS) as part of the NICMOS Guaranteed Time Observer program. NICMOS images, particularly in combination with WFPC2 optical images, have proved to be an effective way to detect dust in the cores of nearby galaxies and have also shown dust to be a common feature of the inner parts of galaxy bulges (Peletier et al. 1999; Quillen, Bower, & Stritzinger 2000; see also van Dokkum & Franx 1995). In this paper, we present these NICMOS observations and their comparison with previous WFPC2 images of both galaxies. Our results generally support existing models of the structures of the cores of both objects and extend the analysis of the infrared emission of these cores to the subarcsecond scale. In the following analysis, we adopt a distance to both galaxies of 784 kpc (Stanek & Garnavich 1998) and a foreground reddening value of $E(B-V) = 0.062$ (Burstein &

Heiles 1982) with an $R_V = 3.1$ extinction curve, noting that this extinction value is very uncertain as a result of the large angular extent of both galaxies.

2. OBSERVATIONS AND REDUCTIONS

2.1. *Data and Basic Reduction*

NICMOS camera 2 images of the cores of M31 and M32 were obtained on UT 1997 December 2 with filters F110W, F160W, and F222M. These filters are similar to the standard *JHK* filters, with central wavelengths and FWHM values of 1.102 and 0.592 μm, 1.593 and 0.403 μm, and 2.216 and 0.143 μm, respectively. The images were taken in the MULTIACCUM mode (which facilitates cosmic-ray rejection) in a four-step spiral dither pattern, with total integration times per filter of 128 s (F110W and F222M) and 64 s (F160W) for both galaxies. The raw images were reduced using a set of "super" flat-field and bias frames obtained from combining large sets of individual flat-field and bias frames obtained on-orbit and nearly contemporaneously with these observations, which should improve their photometric accuracy by several percent compared with the standard "pipeline"-reduced images (see Corbin et al. 2000). Photometric calibration is based on the values for each NICMOS camera and filter determined from observations of standard stars made on-orbit (see Colina & Rieke 1997).[1] Photometric calibration of the WFPC2 images is based on the conversion factors from counts to fluxes given in the image headers. Image orientations (degrees by which *y*-axes of images are rotated east of north) are $-140\overset{\circ}{.}48$ (M31) and $-132\overset{\circ}{.}98$ (M32).

2.2. *Point-spread Function Issues*

Of primary importance in the analysis of these data is the treatment of the image point-spread functions (PSFs). Because NICMOS images are diffraction limited, the image PSFs are strongly dependent on wavelength, with, for example, the PSF of the F222M images being approximately twice as wide as that of the F110W images. Optimally, one wishes to deconvolve the PSFs for each filter to bring the images into maximum sharpness, as was done for the WFPC2 images of L98. However, our attempts to deconvolve the present NICMOS images failed, in that the deconvolved images contained structure that was likely to be artificial, such as amplified image noise, as opposed to real features in the objects. Specifically, we used images of isolated stars obtained near in time to (but not contemporaneous with; no PSF stars were specifically observed for this program) the observations of both galaxies, as well as artificial PSF images produced by the Tiny Tim program (Krist & Hook 1999),[2] as inputs for the deconvolution programs (both Lucy-Richardson and maximum entropy method) available in IRAF. In all cases the results were similar, in that the "deconvolution" introduced spurious features (e.g., halos around individual stars) into the output images. We attribute this failure to several factors, including the differences in detector focus between the object and PSF star observations, the different placement of the PSF star on the detector relative to the galaxy nuclei (which are our main features of interest), and pixel-to-pixel variations in the actual PSFs that are not matched in the Tiny Tim images. Also, even slight undersampling of the PSF in each band (which can occur for NICMOS camera 2 in F110W) can lead to mismatches between the object and input PSFs, as well as the introduction of photometric errors (see Lauer 1999).

For the purpose of producing composite images of the galaxies in the NICMOS filters, we therefore chose to combine the original, i.e., nondeconvolved, F110W, F160W, and F222M images, in order to obtain the highest image resolution. However, the symmetry of the M32 core allows us to examine the radial color profiles derived from the NICMOS images. To maximize the accuracy of these colors for the M32 NICMOS images, we thus first lowered the resolution of the F110W and F160W images to that of the F222M image by applying (flux-conserving) Gaussian convolution. Three difference images, F110W − F160W, F110W − F222M, and F160W − F222M, were then formed. The asymmetry of the M31 core does not allow a measurement of its radial color profiles, so no convolution was applied to its individual NICMOS images.

For the comparison of WFPC2 and NICMOS images, we chose to examine the F555W − F160W colors of both galaxies, as this color appears to be a good indicator of dust (Quillen et al. 2000). We use the deconvolved F555W images obtained by L98 (kindly provided by T. Lauer), assuming that these images are more accurate than convolved ones. The F160W images used are the original ones, i.e., without convolution to the resolution of the F222M images. To form the F555W − F160W images requires matching the plate scales and PSFs of the separate images. To do this, we first resampled the F555W images to the same pixel scale as the F160W images using sinc function interpolation, and then we convolved them with Tiny Tim PSF images for the F160W filter, created separately for each galaxy. These synthetic PSF images were created taking into account the specific NICMOS focus at the time of observation, the position of the galaxy center on the NICMOS detector, and the orientations of the respective cameras. The resulting F555W images are thus matched to the F160W images as well as possible, although as will be shown in the next section, this matching was imperfect and left small residual features in the F555W − F160W difference images. These difference images were also found to show approximately linear gradients of a few tenths of a magnitude across the central few arcseconds of both galaxies, which at least in the case of M32 is inconsistent with the results of L98 and ground-based data (Michard & Nieto 1991; Bendinelli et al. 1992; Peletier 1993). This gradient could also be a result of the imperfect PSF matching, as well as differences in the image sensitivity levels. The F555W − F160W images are consequently useful primarily as qualitative indicators of the optical/infrared colors and dust content of the cores of both galaxies.

3. RESULTS

3.1. *M31*

A false-color composite image of the F110W, F160W, and F222M images of M31 is shown in Figure 1. In both these images and those for M32, little flux was detected beyond $\sim 5''$ from the galaxy nuclei, so for both galaxies we

[1] See also http://www.stsci.edu/instruments/nicmos.
[2] See http://www.stsci.edu/software/tinytim.

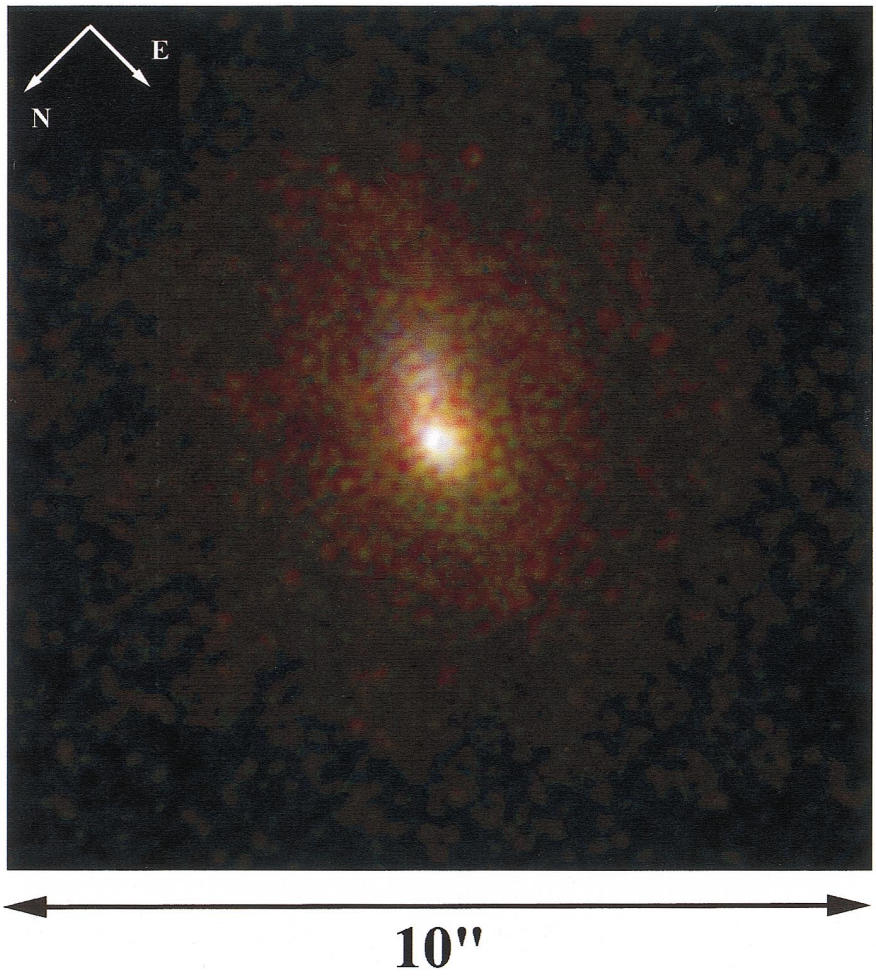


FIG. 1.—False-color composite image of the F110W, F160W, and F222M images of M31, where the images have been assigned to the blue, green, and red color channels, respectively.

show only the inner 10″ × 10″ of the full 19.″2 × 19.″2 camera 2 field. Contour plots of the individual NICMOS images are shown in Figure 2, with the corresponding flux levels given in the figure legend. In Figure 3, we present the F555W−F160W color image, created from the resampled and convolved F555W image as described in the previous section. The F555W and F160W images were aligned to within 0.1 pixels, under the assumption that the peak of the

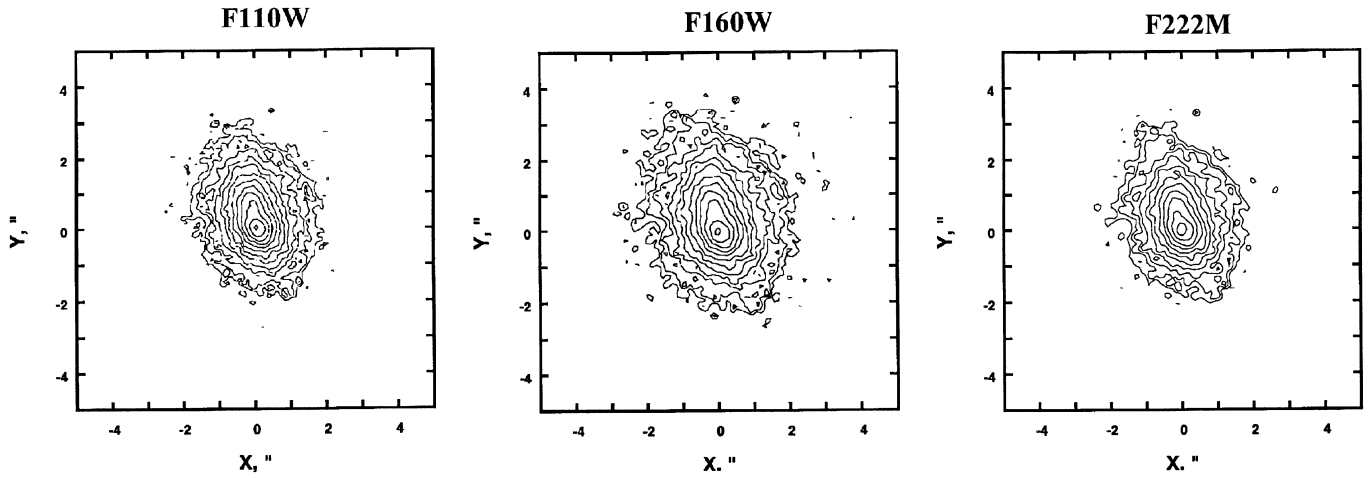


FIG. 2.—Contour plots of the F110W, F160W, and F222M images of M31. Image orientation is the same as in Fig. 1. The intensity scale is logarithmic, and the contour intervals are 0.1 dex. The peak log f_λ (ergs s^{-1} cm^{-2} Å^{-1}) values are −16.15 (F110W), −16.30 (F160W), and −16.50 (F222M).

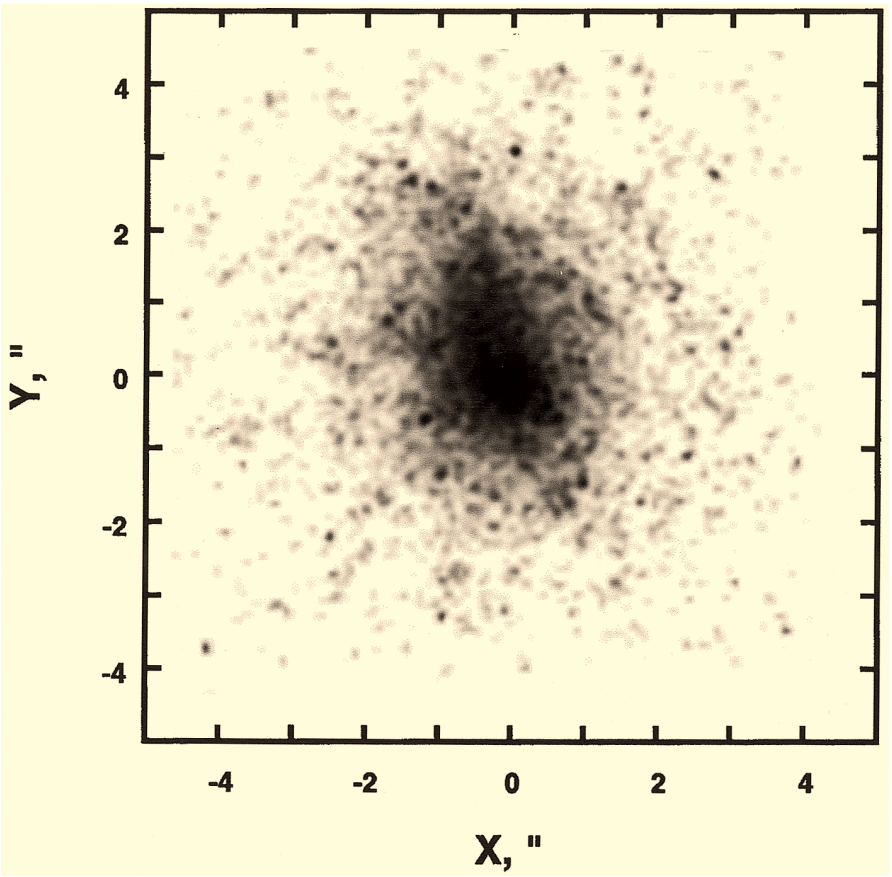


FIG. 3.—A F555W − F160W color image of M31. Image orientation is the same as in Fig. 1. Darker shades indicate redder colors. The faint rings seen around some of the individual stars are the result of the imperfect matching of the image PSFs.

brighter nucleus (P1) occurs at the same physical location in the galaxy at both wavelengths. The imperfect matching of the PSFs of the respective images is evident in the very faint rings seen around some of the individual stars, but the associated difference in flux between these features and the PSF cores is less than 10%.

The basic asymmetry of the nucleus seen in the WFPC2 images and also in ground-based infrared images (Mould et al. 1989) is confirmed in these data. This supports the results of Lauer et al. (1993) and King et al. (1995) and the spectroscopic studies cited in § 1 that the separation of the nucleus into two peaks is not the result of a band of dust crossing a single nucleus. In particular, Figure 3 reveals no distinct dust band similar to those found in some objects in the F555W − F160W images of Peletier et al. (1999) and Quillen et al. (2000), and thus any dust in the vicinity of the core is diffuse. The lack of a distinct peak at P2 in these images (in contrast to the WFPC2 images) is likely due to their relatively lower resolution and depth. By contrast, the lack of evidence for the UV-bright cluster at the edge of P2 discovered by L98 is more likely due to its faintness at these wavelengths. The NICMOS images thus follow the trend of the WPFC2 images, with the ultraviolet source fading away at longer wavelengths.

Although as noted in § 2.2 colors measured from the F555W − F160W images should be treated with caution, for M31 these colors fall in the approximate range 4.0–5.1, which is most consistent with a population dominated by M giant stars (using the tables of Tokunaga 2000, and noting that F555W − F160W $\simeq V-H$). The reddest values ($\simeq 5$) are found at P1. This is consistent with the spectroscopic results of Kormendy & Bender (1999), who find that the stellar populations of P1 and P2 can be acceptably fitted with an M3 III star spectrum, although a better fit is obtained by a composite G8 V and K2 III star spectrum. The resolved stars outside of the central $\sim 1''$ of the core have colors consistent with the approximate spectral range M3–M4. We present the positions and colors of the brightest and best resolved of these stars in Table 1, along with magnitude values in the F160W filter measured from simple aperture photometry. At our adopted distance to M31, these stars have absolute F555W magnitudes also consistent with M giants and occur over projected distances of ~ 4 to 12 pc from the center of P1. We return to a discussion of the possible significance of these stars in § 4.

3.2. *M32*

Our false-color composite NICMOS image of M32 is shown in Figure 4. The difference in filter PSFs is seen more strongly here than in the M31 image, with, specifically, the red ring at $\sim 3''$ from the strongly peaked nuclear emission being an artifact of the wider PSF of the F222M image. Figure 5 shows the contour plots of the original NICMOS images, and Figure 6 shows the F555W − F160W difference image. As in M31, there is no clear evidence of clumps or bands of dust, a result also found by L98. Despite the resolution of some of the individual stars, the NICMOS images are too crowded for batch photometry, which is also

TABLE 1

J2000 COORDINATES, MAGNITUDES, AND COLORS OF M GIANT STARS DISCOVERED NEAR THE M31 NUCLEI

α (00^h42^m) (s)	δ ($+41°16'$) (arcsec)	m(F160W)	m(F555W) − m(F160W)
44.19.....	7.55	18.8	4.6
44.21.....	10.11	19.0	4.4
44.22.....	7.36	18.7	4.6
44.27.....	6.24	19.2	4.6
44.27.....	9.40	18.4	4.7
44.38.....	10.12	18.2	4.8
44.41.....	5.73	19.1	4.5
44.65.....	9.00	18.7	4.7
44.69.....	8.30	19.6	4.5

NOTE.—Coordinates are subject to the roughly $\pm 0\farcs5$ positional uncertainty in *HST* pointing. Relative astrometry can be obtained from the centroid of P1 in these observations: $\alpha = 00^h42^m44^s.42$, $\delta = +41°16'9\farcs25$. Magnitudes and colors are on a Vega scale and have respective uncertainties of ± 0.2 and ± 0.4.

unwarranted because of the variation in the PSF across the detector. However, batch photometry has been obtained from *HST* images of the less crowded outer regions of the galaxy (within $\sim 1'$ of the nucleus) by Grillmair et al. (1996), and to within $\sim 2''$ in the ultraviolet by Brown et al. (1998, 2000). Davidge et al. (2000) have also resolved stars to within $2''$ of the nucleus in H and K using adaptive optics on the Gemini North Telescope.

In Figure 7, we present the F110W − F160W, F110W − F222M, and F160W − F222M color profiles of the inner $4''$ of M32, averaged within annuli of $0\farcs2$ width (approximately equal to the image resolutions) and measured from the centroid of the nucleus. Because batch photometry is not feasible, these profiles were formed by taking the ratios of the respective images. A correction for Galactic extinction has also been applied, assuming the aforementioned reddening value.

The constancy of the NICMOS image color profiles to the scale of the image PSFs is consistent with the results of Peletier (1993), who found such constancy in the $H-K$ color out to a distance of $\sim 10''$ from the nucleus but was limited by seeing to distances greater than $1\farcs5$. His $J-K$ color shows a possible small gradient within $\sim 3''$ from the nucleus that is inconsistent with our result. The NICMOS colors still agree well with the corresponding $J-K$ and $H-K$ colors of Peletier (1993) at the same distances, once the differences between the NICMOS and JHK filter systems are accounted for, and also with the $H-K$ colors of individual stars reported by Davidge et al. (2000). The

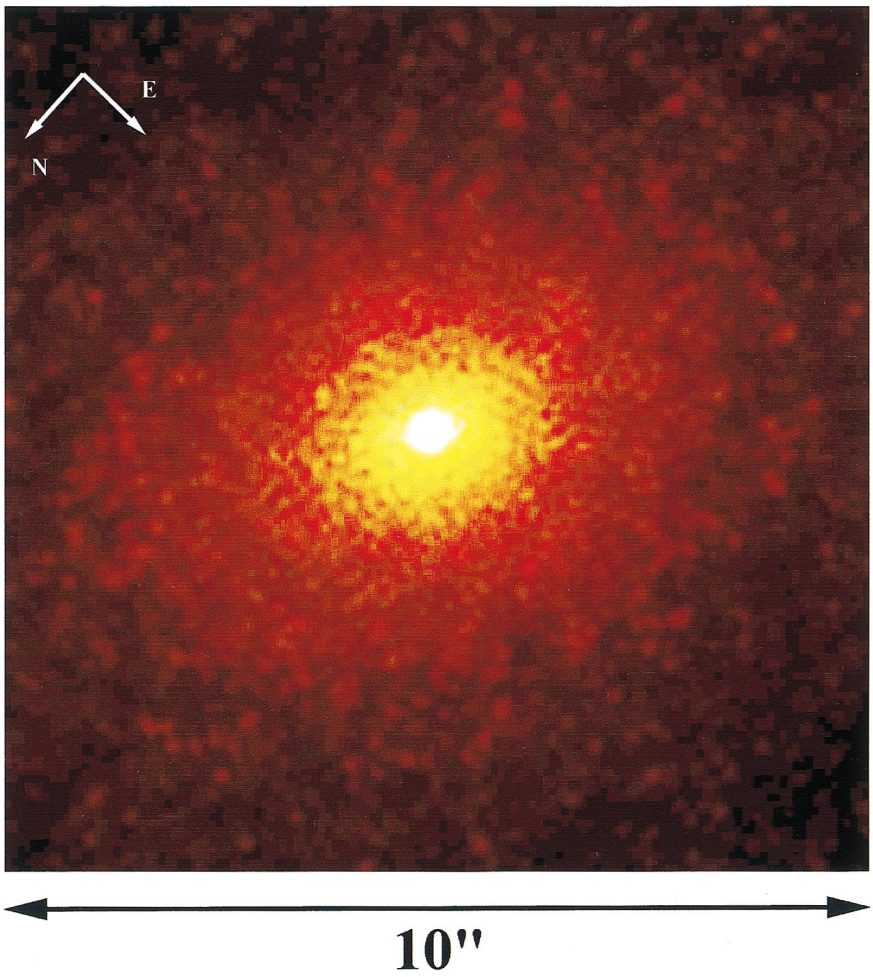


FIG. 4.—Same as Fig. 1, but for M32. The faint red ring at $\sim 3''$ from the nucleus is an artifact of the wider PSF of the F222M filter compared with the F110W and F160W filters.

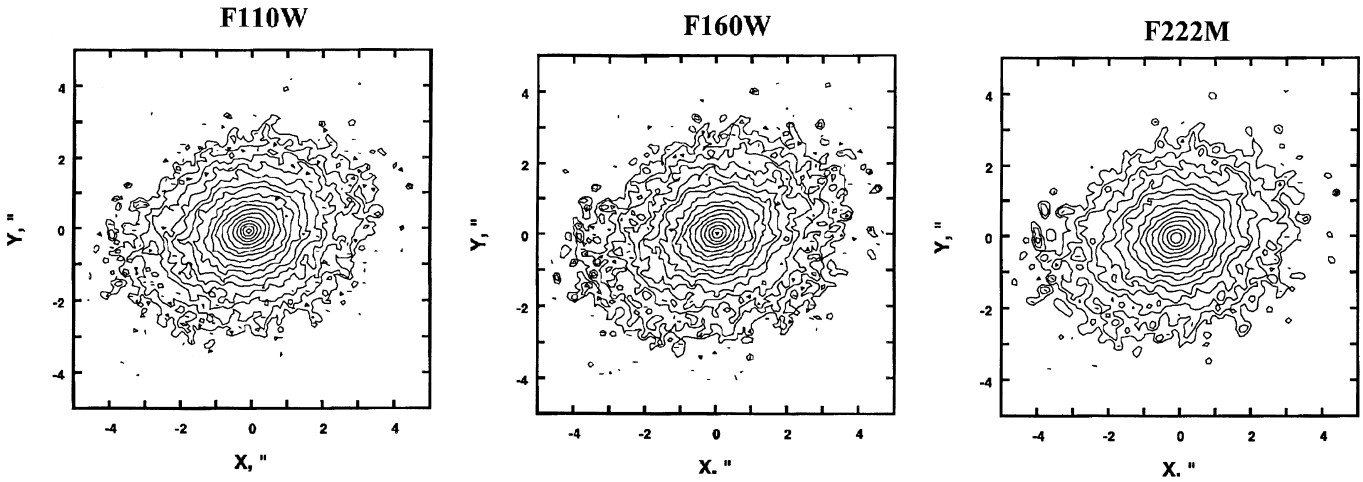


FIG. 5.—Contour plots of the F110W, F160W, and F222M images of M32. Image orientation is the same as in Fig. 4. The intensity scale is logarithmic, and the contour intervals are 0.1 dex. The peak log f_λ (ergs s^{-1} cm^{-2} Å^{-1}) values are -15.60 (F110W), -15.77 (F160W), and -16.16 (F222M).

specific values of all colors measured fall in the range of giant stars of approximate spectral type K3–K5, based on the tables of Tokunaga (2000). This is consistent with the conclusion of del Burgo et al. (2001) from optical spectroscopy of the same region that dwarf stars contribute only up to $\sim 30\%$ of the light in the near-infrared.

L98 find that the core of M32 has a brightness profile that can be fitted by an analytic function (the "Nuker" law) that effectively reduces to a single power-law function at very small distances ($\sim 1''$) from the nucleus. In Figure 8, we present the brightness profiles of the inner $1''$ of M32 in the NICMOS images, in comparison with those for the WFPC2 F555W and F814W filters, where the latter have been resampled to the NICMOS camera 2 pixel scale. These have been plotted on a semilog scale to facilitate comparison between the WFPC2 and NICMOS images. We present

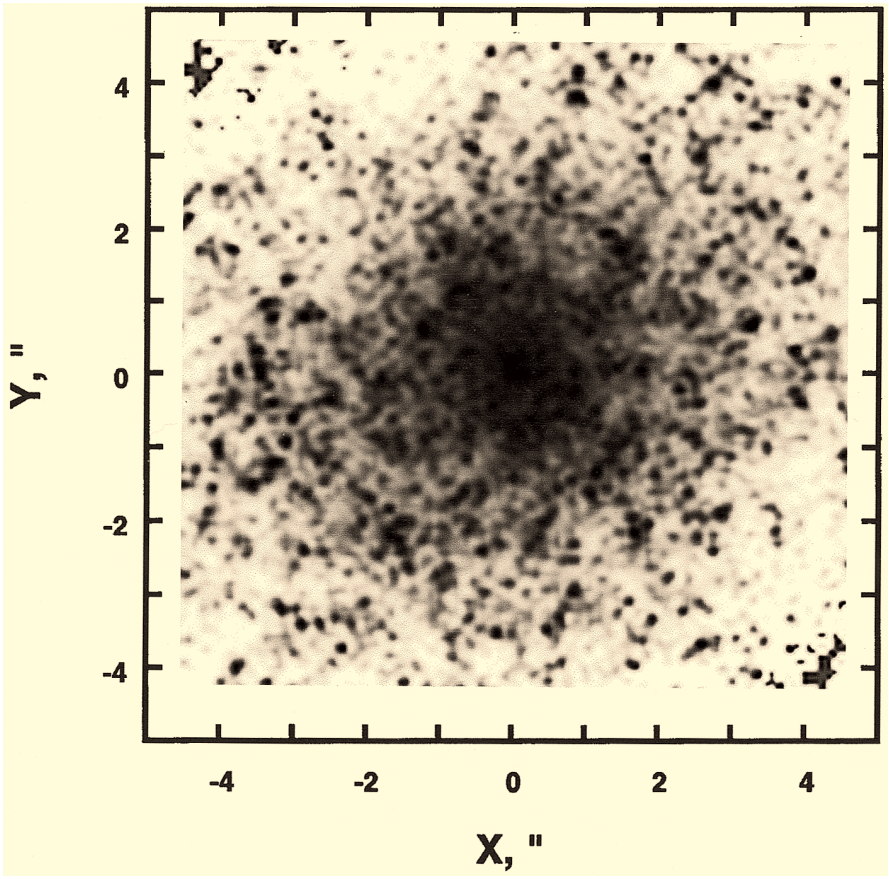


FIG. 6.—A F555W – F160W color image of M32. Image orientation is the same as in Fig. 4.

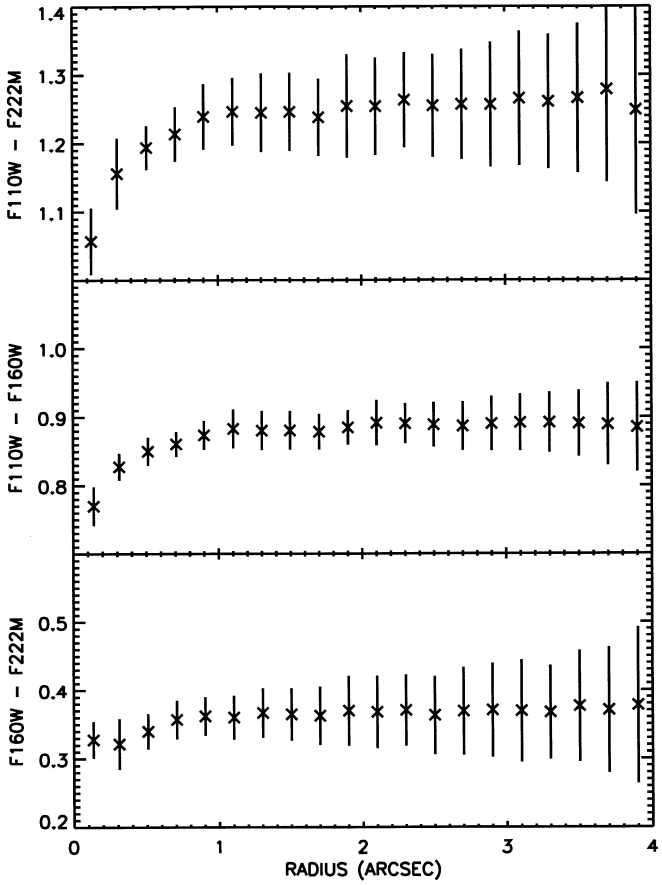


FIG. 7.—NICMOS color profiles of the inner 4″ of M32. Values are on a Vega magnitude scale and represent averages within concentric circular annuli of 0.″2 from the nucleus. Error bars represent the standard deviation of individual pixel values within each annulus. The downturns in the colors at approximately 0.″3 from the center are the result of differences in the filter PSFs.

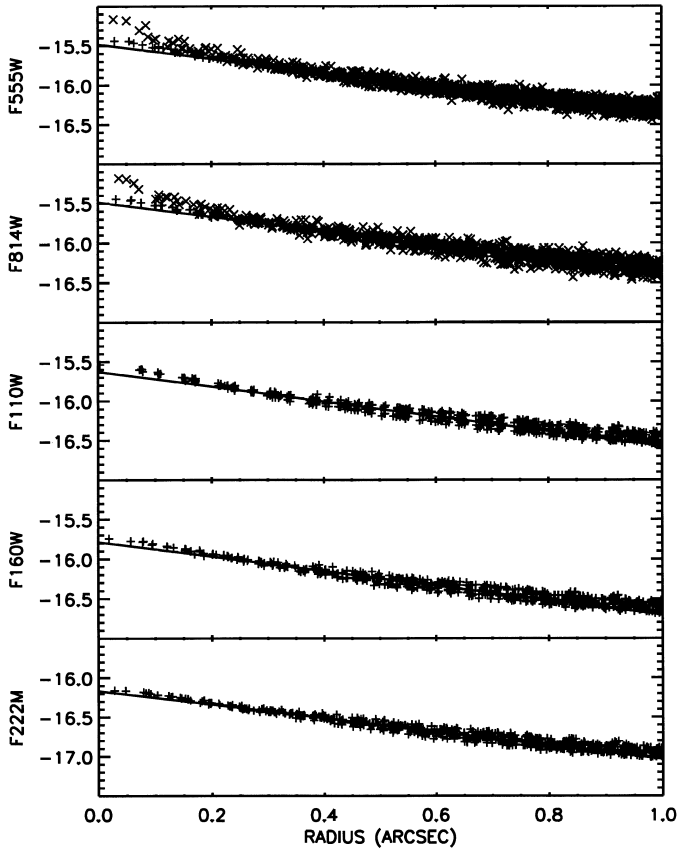


FIG. 8.—Brightness profiles of the inner 1″ of M32 in the WFPC2 F555W and F814W filters and the NICMOS F110W, F160W, and F222M filters. The vertical axis is in units of $\log f_\lambda$ (ergs s^{-1} cm^{-2} $Å^{-1}$). For the WFPC2 images, the plus signs represent the images that have been convolved with the NICMOS F160W filter PSF, while the crosses represent the deconvolved images. The solid lines are linear approximations to the best-fitting power-law functions of the form $f_\lambda \propto r^a$ over the range 0.″2 to 0.″7 from the nucleus and, in the case of the WFPC2 images, represent the fits to the convolved images.

both the brightness profiles of the deconvolved F555W and F814W images of L98 and those from versions of the images that have been convolved with the Tiny Tim NICMOS F160W filter PSF, as discussed in § 2, in order to make their resolutions comparable. We find that the brightness profiles of both the WFPC2 and NICMOS images can be well fitted by a power-law form at distances between approximately 0.″2 and 0.″7 from the nucleus. A linear approximation to these power-law fits has been included in Figure 8 to aid the eye in comparing the WFPC2 and NICMOS images. Using both linear and nonlinear least-squares fitting procedures, we find that the power-law indices for all three NICMOS images and the convolved WFPC2 images differ by no more than 6% from a mean value of approximately $a = -0.91$ (± 0.05), where $f_\lambda \propto r^a$ with r the distance in arcseconds from the nucleus. This index is comparable to the value of -1.2 found by Bendinelli et al. (1992) from seeing-deconvolved ground-based images, and when measured over the same distance range from the nucleus, our values match theirs to within the uncertainties. This result also indicates that the emission in the respective bands is dominated by the same stars, or at least by stars following the same density profile, and further argues against any dust having a strong effect on the optical brightness profiles. There are no clear indications of non-stellar emission in the nucleus in either the WFPC2 images (L98) or the NICMOS images, at least to within the respective resolution limits.

4. DISCUSSION

4.1. *M31*

Our results generally support the currently favored model of Tremaine (1995) that the two nuclei of M31 represent nodes of an eccentric disk of stars with a $\sim 3 \times 10^7$ $M_\odot$ black hole at their dynamical center. The NICMOS images confirm that P1 and P2 are not the result of a thick dust band artificially dividing a single nucleus into two peaks, nor is there evidence that the location of these nuclei changes with wavelength because of a more diffuse dust component, although the presence of a moderate amount of diffuse dust is not excluded by the present data.

The more open question at this point is the nature of the UV-bright cluster, and its relation to the central black hole. Kormendy & Bender (1999) favor this cluster as being the location of the hole on the basis of their kinematic data, a result that would also seem to agree with the spectroscopic results of Statler et al. (1999). This would suggest that the strong ultraviolet emission associated with this cluster is due at least in part to accretion onto the hole. Surrounding stars could be heated by and reflecting the emission of

such an accretion disk, making them bluer, although this hypothesis requires more detailed modeling. Recent X-ray observations of M31's core with the *Chandra* observatory (Garcia et al. 2000) unfortunately do not resolve this issue, because while a strong compact point source is detected near this cluster, its positional uncertainty ($\sim 1''$) is much larger than that of the *HST* images. Nonetheless, if weak accretion onto the central black hole dominates the emission from this source, it would alleviate the dynamical problems associated with the formation of a cluster consisting only of early-type stars, as discussed by L98. Very narrow slit spectroscopy of this source with the Space Telescope Imaging Spectrograph (STIS) would be the best way to distinguish between the stellar cluster and black hole accretion models.

Regarding the M giants listed in Table 1, Kormendy & Bender (1999) have suggested that some stars may escape from the P1/P2 disk and have their orbits phase-mix around the associated center of mass. These M giants are candidates for such escaped stars, given their proximity to the disk and the similarity of their colors to the stars within it. Alternatively, they could be stars in the M31 bulge seen along the line of sight to the nucleus, and thus not dynamically associated with the P1/P2 disk. Kinematic data on these stars, obtainable with 8 m class telescopes under excellent seeing, could help resolve this issue. Specifically, if the stars have escaped from the disk, they would have velocities comparable to the largest seen in the disk itself, ~ 300 km s^{-1}, while the velocities of stars in the halo should be lower. Unfortunately, such velocities are still too low to produce measurable proper motions of the stars at the adopted distance to M31 over observationally feasible timescales.

4.2. *M32*

Del Burgo et al. (2001) find no significant gradient in the strength of key absorption lines such as Hγ, Hβ, and the infrared Ca II triplet from ground-based multiaperture spectroscopy of the same region covered by our images. In combination with this result, the constancy of our infrared color profiles (Fig. 7), as well as those of Peletier (1993) and the small dispersion in the $H-K$ colors of resolved stars found by Davidge et al. (2000), supports the interpretation that the core of M32 has a relatively homogeneous stellar population. Del Burgo et al. conclude that this population can be modeled as being coeval and of intermediate age (~ 4 Gyr) with a metallicity comparable to solar ($Z = 0.02$), which is consistent with the result that the infrared colors of this population match those of K giants. In addition to the absence of any obvious dust features revealed in our F555W $-$ F160W image, the similarity of the brightness profiles in the optical and infrared (Fig. 7) argues against a large amount of dust being present in the galaxy and, consequently, affecting the form of the optical brightness profiles. The estimates of Bendinelli et al. (1992) and L98 of a relaxation timescale of ~ 2–3 Gyr for the M32 core based on the form and slope of these brightness profiles would thus appear to remain valid.

Our results and those of L98 indicate that any optical and infrared emission produced by accretion onto the central black hole in the M32 nucleus is very weak or absent. However, the X-ray observations of Eskridge et al. (1996), Lowenstein et al. (1998), and Zang & Meurs (1999), as well as the possible far-ultraviolet excess in the M32 nucleus reported by Ohl et al. (1998), suggest that a low level of accretion is occurring and is best detected at shorter wavelengths. A conclusive test of such a "micro-AGN" model for the nucleus of M32 requires deep pointed X-ray observations with the *Chandra* observatory, such as those made by Garcia et al. (2000) of the center of M31. A deep narrow-slit ultraviolet spectrum of the M32 nucleus with STIS would also be useful in order to see whether weak emission lines are present, and to determine the form of the nuclear continuum.

We thank Tod Lauer for providing us with copies of his WFPC2 images, and for helpful suggestions for the analysis of these data. We additionally thank Alice Quillen and Dean Hines for helpful discussions, Betty Stobie and Howard Bushouse for assistance with the analysis software, and Rick White for discussions of image deconvolution. An anonymous referee also provided important comments that improved the paper. This work was supported by NASA grant NAG 5-3042 to the University of Arizona. This work has also made use of the NASA Extragalactic Database, which is operated by the Jet Propulsion Laboratory under contract with NASA.

REFERENCES

Bendinelli, O., Parmeggiani, G., Zavatti, F., & Djorgovski, S. 1992, AJ, 103, 110
Brown, T. M., Bowers, C. W., Kimble, R. A., Sweigert, A. V., & Ferguson, H. C. 2000, ApJ, 532, 308
Brown, T. M., Ferguson, H. C., Stanford, S. A., & Deharveng, J.-M. 1998, ApJ, 504, 113
Burstein, D., & Heiles, C. 1982, AJ, 87, 1165
Colina, L., & Rieke, M. J. 1997, in The 1997 *HST* Calibration Workshop, ed. S. Casertano, R. Jedrzejewski, C. D. Keyes, & M. Stevens (Baltimore: STScI), 182
Corbin, M. R., Vacca, W. D., O'Neil, E., Thompson, R. I., Rieke, M. J., & Schneider, G. 2000, AJ, 119, 1062
Davidge, T. J., Rigaut, F., Chun, M., Brandner, W., Potter, D., Northcott, M., & Graves, J. E. 2000, ApJ, 545, L89
del Burgo, C., Peletier, R. F., Vazdekis, A., Arribas, S., & Mediavilla, E. 2001, MNRAS, 321, 227
Eskridge, P. B., White, R. E., III, & Davis, D. S. 1996, ApJ, 463, L59
Garcia, M. R., Murray, S. S., Primini, F. A., Forman, W. R., McClintock, J. E., & Jones, C. 2000, ApJ, 537, L23
Grillmair, C. J., et al. 1996, AJ, 112, 1975
King, I. R., Stanford, S. A., & Crane, P. 1995, AJ, 109, 164
Kormendy, J., & Bender, R. 1999, ApJ, 522, 772
Krist, J., & Hook, R. 1999, The Tiny Tim User's Guide (version 5.0; Baltimore: STScI)
Lauer, T. R. 1999, PASP, 111, 1434
Lauer, T. R., Faber, S. M., Ajhar, E. A., Grillmair, C. J., & Scowen, P. A. 1998, AJ, 116, 2263 (L98)
Lauer, T. R., et al. 1993, AJ, 106, 1436
Lowenstein, M., Hayashida, K., Toneri, T., & Davis, D. S. 1998, ApJ, 497, 681
Michard, R., & Nieto, J.-L. 1991, A&A, 243, L17
Mould, J., Graham, J., Matthews, K., Soifer, B. T., & Phinney, E. S. 1989, ApJ, 339, L21
Ohl, R. G., et al. 1998, ApJ, 505, L11
Peletier, R. F. 1993, A&A, 271, 51
Peletier, R. F., Balcells, M., Davies, R. L., Andredakis, Y., Vazdekis, A., Burkert, A., & Pravda, F. 1999, MNRAS, 310, 703
Quillen, A. C., Bower, G. A., & Stritzinger, M. 2000, ApJS, 128, 85
Stanek, K. Z., & Garnavich, P. M. 1998, ApJ, 503, L131
Statler, T. S., King, I. R., Crane, P., & Jedrzejewski, R. I. 1999, AJ, 117, 894
Tokunaga, A. 2000, in Allen's Astrophysical Quantites, ed. A. N. Cox (4th ed.; New York: Springer), 152
Tremaine, S. 1995, AJ, 110, 628
van der Marel, R. P., Cretton, N., de Zeeuw, P. T., & Rix, H.-W. 1998, ApJ, 493, 613
van der Marel, R. P., de Zeeuw, P. T., & Rix, H.-W. 1998, ApJ, 488, 119
van Dokkum, P. G., & Franx, M. 1995, AJ, 110, 2027
Zang, Z., & Meurs, E. J. A. 1999, NewA, 4, 521